



# Digitally switchable multi-focal lens using freeform optics

XUAN WANG,<sup>1</sup> YI QIN,<sup>1</sup> HONG HUA,<sup>1,\*</sup> YUN-HAN LEE,<sup>2</sup> AND SHIN-TSON WU<sup>2</sup>

<sup>1</sup>3D Visualization and Imaging Systems Laboratory, College of Optical Science, The University of Arizona, 1630 E University Blvd., Tucson, AZ 85721, USA

<sup>2</sup>CREOL, The College of Optics and Photonics, University of Central Florida, Orlando, FL 32816, USA

\*hhua@optics.arizona.edu

**Abstract:** Optical technologies offering electrically tunable optical power have found a broad range of applications, from head-mounted displays for virtual and augmented reality applications to microscopy. In this paper, we present a novel design and prototype of a digitally switchable multi-focal lens (MFL) that offers the capability of rapidly switching the optical power of the system among multiple foci. It consists of a freeform singlet and a customized programmable optical shutter array (POSA). Time-multiplexed multiple foci can be obtained by electrically controlling the POSA to switch the light path through different segments of the freeform singlet rapidly. While this method can be applied to a broad range of imaging and display systems, we experimentally demonstrate a proof-of-concept prototype for a multi-foci imaging system.

© 2018 Optical Society of America under the terms of the [OSA Open Access Publishing Agreement](#)

**OCIS codes:** (120.4820) Optical systems; (220.3620) Lens system design; (220.1250) Aspherics; (230.3720) Liquid-crystal devices.

## References and links

1. M. J. Moghimi, B. J. Lutzenberger, B. M. Kaylor, and D. L. Dickensheets, "MOEMS deformable mirrors for focus control in vital microscopy," *J. Micro. Nanolithogr. MEMS MOEMS* **10**(2), 023005 (2011).
2. M. Kang and R. Yue, "Variable-focus liquid lens based on EWOD," *J. Adhes. Sci. Technol.* **26**(12–17), 1941–1946 (2012).
3. S. T. Choi, J. Y. Lee, J. O. Kwon, S. Lee, and W. Kim, "Liquid-filled varifocal lens on a chip," in *MOEMS and Miniaturized Systems VIII. Vol. 7208* (ISOP, 2009).
4. S. Suyama, M. Date, and Hi. Takada, "Three-dimensional display system with dual-frequency liquid-crystal varifocal lens," *Jpn. J. Appl. Phys.* **39**(2R), 480 (2000).
5. S. H. Lu and H. Hua, "Structured illumination assisted microreflectometry with optical depth scanning capability," *Opt. Lett.* **41**(17), 4114–4117 (2016).
6. S. Liu and H. Hua, "Extended depth-of-field microscopic imaging with a variable focus microscope objective," *Opt. Express* **19**(1), 353–362 (2011).
7. S. H. Lu and H. Hua, "Imaging properties of extended depth of field microscopy through single-shot focus scanning," *Opt. Express* **23**(8), 10714–10731 (2015).
8. F. O. Fahrbach, F. F. Voigt, B. Schmid, F. Helmchen, and J. Huisken, "Rapid 3D light-sheet microscopy with a tunable lens," *Opt. Express* **21**(18), 21010–21026 (2013).
9. Y. Qin and H. Hua, "Continuously zoom imaging probe for the multi-resolution foveated laparoscope," *Biomed. Opt. Express* **7**(4), 1175–1182 (2016).
10. Y. Zou, W. Zhang, F. S. Chau, and G. Zhou, "Miniature adjustable-focus endoscope with a solid electrically tunable lens," *Opt. Express* **23**(16), 20582–20592 (2015).
11. E. J. Tremblay, I. Stamenov, R. D. Beer, A. Arianpour, and J. E. Ford, "Switchable telescopic contact lens," *Opt. Express* **21**(13), 15980–15986 (2013).
12. H. Hua, "Enabling focus cues in head-mounted displays," *Proc. IEEE* **105**(5), 805–824 (2017).
13. S. Liu, H. Hua, and D. Cheng, "A novel prototype for an optical see-through head-mounted display with addressable focus cues," *IEEE Trans. Vis. Comput. Graph.* **16**(3), 381–393 (2010).
14. S. Liu and H. Hua, "Time-multiplexed dual-focal plane head-mounted display with a liquid lens," *Opt. Lett.* **34**(11), 1642–1644 (2009).
15. G. D. Love, D. M. Hoffman, P. J. Hands, J. Gao, A. K. Kirby, and M. S. Banks, "High-speed switchable lens enables the development of a volumetric stereoscopic display," *Opt. Express* **17**(18), 15716–15725 (2009).
16. X. Hu and H. Hua, "High-resolution optical see-through multi-focal-plane head-mounted display using freeform optics," *Opt. Express* **22**(11), 13896–13903 (2014).

17. Y. H. Lee, F. Peng, and S. T. Wu, "Fast-response switchable lens for 3D and wearable displays," *Opt. Express* **24**(2), 1668–1675 (2016).
18. Optotune, Inc., "Fast electrically tunable lens EL-16-40-TC," <http://www.optotune.com/products/focus-tunable-lenses/electrical-lens-el-16-40-tc>.
19. J. W. Goodman, *Introduction to Fourier Optics*, 2nd ed. (McGraw-Hill, 1996), Chap. 4.
20. M. Xu and H. Hua, "High dynamic range head mounted display based on dual-layer spatial modulation," *Opt. Express* **25**(19), 23320–23333 (2017).

## 1. Introduction

An optical device that offers the capability of electrically controlling or tuning its optical power without mechanically moving parts is commonly referred to as a tunable lens or varifocal element (VFE) interchangeably. Typically, by applying different driven signals, voltage mostly, the optical power of an VFE can be controlled through either modifying the shape of a refractive or reflective surface of the element or varying the refractive index of the material. Examples include deformable membrane mirror device (DMMD) [1], electrowetting lens [2], elastomer-membrane fluidic lens [3], and liquid crystal lens [4]. An VFE can find a broad range of applications in many fields, from head-mounted displays for virtual and augmented reality (VR/AR) applications, vision correction, to 3D microscopy. For instance, in 3D microscopy, VFEs enables flexible, extended depth of field volume imaging at high speeds without the need of mechanically moving the specimen or objective [5–8]. In Endoscopy, VFEs enable the development of multi-resolution foveated laparoscopes for safer minimally invasive surgery [9] and enable the development of a miniature adjustable-focus endoscope [10]. In vision correction, Tremblay *et al.* demonstrated a contact lens switchable between normal and magnified vision using the polarization property of liquid crystals [11].

In recent years, the VFE technology has been identified as one of the key enabling technologies in creating accurate focus cues in head-mounted displays for the rapidly emerging VR and AR applications [12]. It is especially useful in addressing the accommodation and convergence conflict in conventional stereoscopic 3D displays by dynamically varying the focal depth of the display in accordance to a viewer's depth of interest [13] or rapidly rendering multiple image planes at different focal distances to create light field true 3D displays [14–17]. For instance, Suyama *et al.* demonstrated a dual-focal-plane display using a dual-frequency liquid-crystal varifocal lens [4]. Liu and Hua presented a dual-focal plane display prototype with addressable focal distances throughout a volumetric space from 0 to 8 diopters enabled by a liquid lens device [14]. Love *et al.* developed a four-focal-plane prototype with discrete addressable focal planes enabled by birefringence lenses [15]. Hu and Hua demonstrated a depth-fused six focal plane prototype utilizing a deformable membrane mirror device (DMMD) as the tunable optics [16].

None of the state-of-the-art electrically controlled VFE technologies, however, can fully meet the requirements of high-speed, large aperture, large range of tunable power, low-voltage control, robustness, and compactness, which are necessary properties for creating a wearable display solution. For example, the DMMD technology by OKO can offer an adequately high speed of over 1 KHz, but it has a small range of varying optical power (about ~1.2 diopters) and a limited optical aperture of less than 10 mm, which lead to necessary tradeoffs between tunable depth range and system exit pupil diameter due to the Lagrange invariant constraint [14]. Additionally, the device requires a high driving voltage of about 200 volts, which is inappropriate for a wearable device, and the thin membrane nature of the device is prone to damage. The liquid lens technology based on electrowetting phenomenon [15] offers a large range of tunable optical power and has the desirable refractive nature, but it has a limited response speed of approximately 30-100 Hz and very small optical aperture of about 2.5-4 mm. The electronically tunable lens offered by Optotune Inc. is another emerging technology based on the combination of optical fluids and elastic polymer membrane [18]. It affords a large range of tunable power, low voltage control, the desirable refractive nature, and a large optical aperture (up to 16 mm). However, it requires 6-15 ms for settling, making

the overall speed inadequate. Additionally, the optical power is sensitive to temperature and to gravity. The conventional liquid crystal lenses are subject to slow response speed. Recently, Lee et al. presented a hybrid solution of a switchable lens for 3D display applications, in which twisted nematic liquid crystal was used in combination with conventional lenses [17], and demonstrated the ability to achieve high-speed switching between two focal distances. Although the number of foci can be extended by stacking more sets of liquid crystal modules, the volume will increase and a large range of varying power requires longer path and a large system volume.

In this paper, we present a novel design and prototype of a digitally switchable multi-focal lens (MFL) that offers the capability of rapidly switching the optical power of the system among multiple foci. The switchable MFL consists of a custom-designed freeform singlet and a custom-made high-speed programmable optical shutter array (POSA). The freeform singlet, with a clear aperture diameter of 20mm, consists of four zones, through which four distinct foci are produced. The POSA consists of four corresponding concentric patterns of fast-switching liquid crystal material, which has a rising time of 2.5 ms and a falling time of 0.5 ms. By combining the multi-focal freeform singlet and the POSA in a time-multiplexing fashion, a four-focal plane switchable lens was achieved at an overall switching speed of about 400Hz. Compared to other existing VFE technology, the proposed switchable MFL can afford all the desired properties such as high-speed, large aperture, large range of switchable power, low-voltage control, robustness, compactness, and scalability. A proof-of-concept prototype was built to demonstrate one application of the new switchable lens. The rest of the paper is structured as follows. Section 2 describes the optical design of our proposed solution, section 3 presents the design of a custom shutter array along with the optimization of its apertures for uniform illumination and experimental characterization of the shutter, and section 4 experimentally demonstrates a proof-of-concept multi-focal imaging system utilizing the proposed tunable optics.

## 2. Optical design approach

Figure 1 shows a schematic design of a switchable MFL. As shown in Fig. 1(a), it consists of two key elements: a multi-focal freeform singlet and a POSA. One of the lens surfaces is a freeform shape which is divided into multiple concentric zones along its radial direction, shown in Fig. 1(b). The surface shape varies such that its optical power depends on the ray height incident on the lens, thus the concentric zones create a sequence of distinctive foci (e.g.  $F_1$ ,  $F_2$ ,  $F_3$ ,  $F_4$  etc.). To digitally address the foci, a POSA such as a programmable spatial light modulator (SLM), illustrated in Fig. 1(a), is attached next to the freeform surface of the lens. Its aperture is divided into multiple concentric regions, corresponding to the ray heights of the different foci. The focus of the lens can be rapidly switched among the foci by controlling the light transmission through each concentric region of the aperture array.

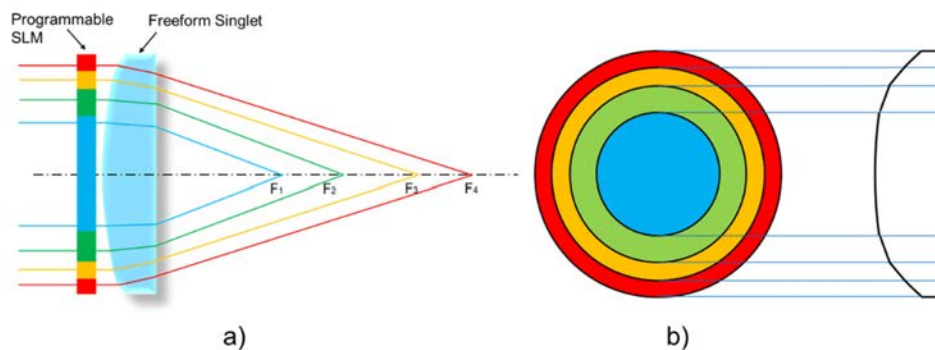


Fig. 1. (a) Four focal planes of the singlet. (b) The profile of the singlet.

Consider the design of a freeform singlet creating  $N$  discrete foci,  $F_1, F_2, \dots$  and  $F_N$ , respectively, arranged in order along the optical axis, where  $F_1$  is the nearest focal point. Without loss of generality, let us assume that the first zone (i.e. center) of the lens corresponds to the nearest focal point,  $F_1$ . One of the critical considerations in designing an MFL singlet is to ensure that the effective numerical aperture of each focal zone remains nearly constant such that the light throughput of an MFL system is independent of the focal distance. To satisfy this requirement, the constraint applied to the focal length and zone radius is expressed as

$$\frac{r_i^2 - r_{i-1}^2}{f_i^2} = \frac{r_1^2}{f_1^2} \quad i = 2, \dots, N \quad (1)$$

Where  $f_i$  is the focal length of the  $i^{\text{th}}$  focal zone of the lens and  $r_i$  is the radial distance of the outer edge of the  $i^{\text{th}}$  focal zone, which is also the radial distance of the inner edge of the  $(i-1)^{\text{th}}$  focal zone. Another key consideration in designing an MFL is to ensure surface continuity at the transition edges between adjacent focal zones such that no gap or transition zone is created during the fabrication process. This constraint can be expressed as

$$z_i(r_{i-1}) = z_{i-1}(r_{i-1}) \quad i = 2, \dots, N \quad (2)$$

Where  $z_i(r)$  denotes the surface sag of the  $i^{\text{th}}$  focal zone of the lens at a given radial position  $r$ .

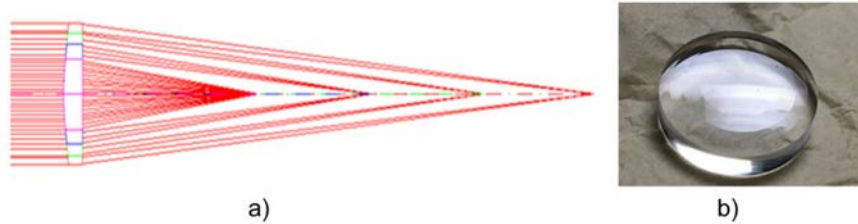


Fig. 2. (a) Optical layout of a MFL design. (b) photograph of our freeform lens prototype.

Based on the method described above, we designed an MFL singlet with a clear aperture of 20 mm in diameter. Figure 2(a) shows the optical layout of the MFL singlet design. The singlet consists of a rotationally symmetric convex surface and a planar surface, where the convex surface was formed by four concentric segments of aspherical surfaces and creates four foci with a focal length of 50 mm, 80 mm, 110 mm and 140 mm, respectively. Each segment of the aspherical surfaces was optimized to use up to 6th order term described as

$$z_i(r) = \frac{r^2}{R_i(1 + \sqrt{1 - (1 + K_i)\frac{r^2}{R_i^2}})} + a_{4,i}r^4 + a_{6,i}r^6 \quad r \in (r_{i-1}, r_i) \quad (3)$$

Where  $R_i$  is the radius of curvature of the  $i^{\text{th}}$  focal zone,  $K_i$  is the conic constant,  $a_{4,i}$  and  $a_{6,i}$  are the aspherical coefficients of 4th and 6th terms.

The outer diameters of the four focal zones are 10 mm, 14.14 mm, 17.32 mm, and 20 mm, respectively. To satisfy the constraint defined in Eq. (2), the vertex of each aspherical surface segment was shifted axially until the surfaces of adjacent focal zones intersect precisely at the radial positions defining the outer edges of each zone. Figure 2(b) shows a photograph of the MFL lens fabricated via a precision diamond turning process and the picture clearly shows the four segments of the convex surface. It is worth noting that this design chose to place the four focal zones in the order of increasing focal lengths from the center to the edge of the lens. This choice has multi-fold benefits. First of all, placing the focal zones of shorter focal lengths near the center leads to a much smaller equivalent numerical aperture for the short-

focal length zones than placing the foci in a reverse order, which makes it easier to balance aberrations. Secondly, the difference between the ray incidence angles on the different surface segments of the MFL focal zones is much smaller compared to when the foci are arranged in a reverse order. This smaller ray angle variation will not only make it easier to design and couple this MFL into optical systems and also reduce crosstalk between adjacent focal zones.

### 3. Custom design of a shutter array

Besides the optical design of a freeform lens creating multiple foci, choosing the appropriate technology and placement for the POSA element is crucial to both the optical performance and response speed of a switchable MFL system. For instance, the response speed of the POSA element directly determines the switchable speed among the focal zones. A minimal spacing between the POSA element and the multi-focal surface is desired to maximize the field of view (FOV) by each focal zone and minimize crosstalk between adjacent zones.

In principle, a straightforward choice is a transmissive-type SLM such as a transmissive liquid crystal display (LCD) on which a sequence of modulation masks as illustrated in Fig. 3 can be rendered sequentially to switch the light transmission through the different focal zones of the MFL singlet. The thin-profile of a typical miniature LCD offers the ability to attach it directly next to the convex surface of the MFL singlet, yielding a compact system with maximal FOV and minimal crosstalk. Furthermore, owing to the pixel array nature of an LCD-type SLM, it offers the ability to flexibly optimize the shape of each modulation mask as needed to balance light throughput of the focal zones and minimize artifacts such as crosstalk between adjacent zones. In practice, however, the usage of an LCD-type SLM suffers from several critical problems, among which the most significant one is the diffraction artifacts introduced by its low-fill factor pixels.

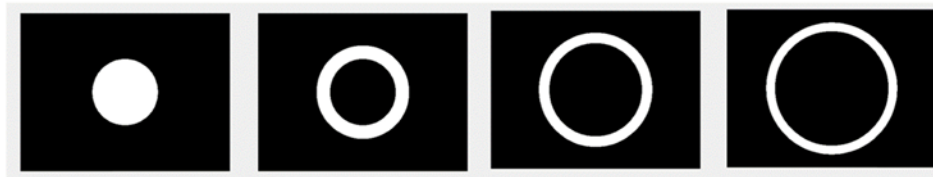


Fig. 3. Modulation mask sequence on an LCD for the four zones of the MFL singlet.

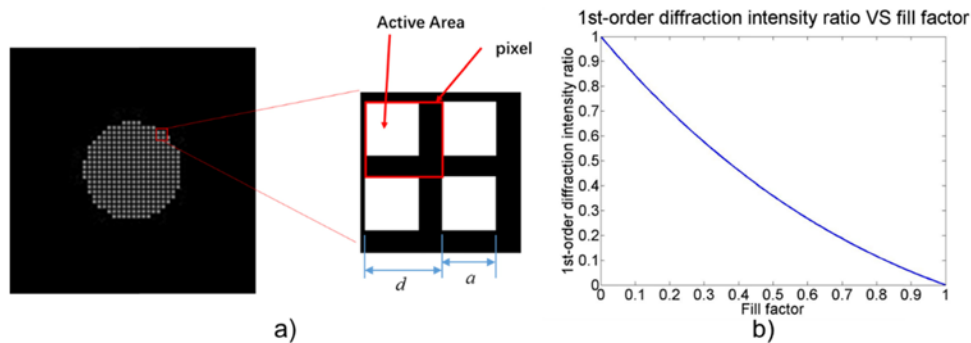


Fig. 4. (a) SLM pixelated aperture model. (b) Relationship between 1st order diffraction intensity ratio and fill factor.

Figure 4(a) illustrates a circular pixelated modulation mask with a radius of  $r_0$  rendered for the central focal zone and the inset image shows the pixel structure of the mask. With the assumption of a square pixel, the fill factor of each pixel,  $\eta$ , is defined as the ratio of the active area to the pixel area, given by

$$\eta = \frac{a^2}{d^2} \quad (4)$$

where  $a$  is the side length of the active pixel area and  $d$  is the pixel pitch. The pupil transmission function of such a pixelated modulation mask can be expressed as

$$P(x, y) = [\text{comb}(\frac{x}{d}, \frac{y}{d}) \times \text{circ}(\frac{x}{r_0}, \frac{y}{r_0})] ** \text{rect}(\frac{x}{a}, \frac{y}{a}) \quad (5)$$

According to Fresnel diffraction theory [19], by applying the Fourier transform to the aperture function defined in Eq. (4), the point spread function of a focus beam through such an aperture can be obtained and expressed as.

$$h(u, v) = [\text{comb}(\frac{du}{\lambda f_1}, \frac{dv}{\lambda f_1}) ** \text{somb}(\frac{r_0 \rho}{\lambda f_1})] \cdot \text{sinc}(\frac{au}{\lambda f_1}, \frac{av}{\lambda f_1}) \quad (6)$$

Where  $f_1$  is the focal length of the incident beam from the central focal zone,  $\lambda$  is the wavelength.

Due to the fact that the aperture radius is much larger than the pixel pitch  $d$  (i.e.  $r_0 \gg d$ ), in Eq. (6), the width of the *Somb* function is far narrower than the *Sinc* function and the sampling interval in comb function. Therefore, the point spread function can be regarded as a sampled *Sinc* function with the sampling interval of  $\Delta = \frac{\lambda f_1}{d}$ . Therefore the intensity ratio of

the 1st order diffraction image to the zero-order is given as  $\text{sinc}^2(\frac{a}{d})$  and decreases as the fill factor of the pixels increases, which was shown in Fig. 4(b). A high fill-factor is desired to minimize the diffraction artifacts caused by a pixelated aperture. Given that the typical fill factor of commercially available transmissive LCD is about 50% or lower, the 1st order diffraction image can have as high as 13.5% image intensity compared to the zero-order ideal image, which leads to significantly reduced image contrast and resolution. Although a reflective-type SLMs such as liquid crystal on silicon (LCoS) devices or digital mirror devices (DMD) offer much higher fill factor, their reflective nature requires enough space gap between the SLM and the MFL to insert a necessary beam splitter for a reflective device, which leads to a significantly reduced FOV and introduces severe crosstalk unless an optical relay may be introduced to the system [20].

To address the diffraction problem introduced by a pixelated aperture array, we custom-designed a circularly-patterned liquid crystal aperture. Figure 5(a) shows the schematic design of a four-zone aperture. Barriers between different zones are needed as electrode gap, which is  $50 \mu\text{m}$  width and can be reduced to as small as  $5 \mu\text{m}$ . A small portion on one side of the aperture is reserved for guiding the electrodes out to connect to the control voltage signal. Figure 5(b) shows the side view of the device construction. The liquid crystal and two transparent electrode layers are sandwiched between the two glass substrates. Two orthogonal polarizers are separately attached to the outer surface of each glass substrate. In general, the liquid crystal layer is several microns thick and the thickness of the electrode layer can also be submicron. Therefore, the thickness of the device will mainly depend on the glass substrate and polarizers. The glass substrate we used is about 1.1 mm thick and the thickness of the polarizer is about  $225 \mu\text{m}$ , which makes the device a total thickness of about 2.65 mm.

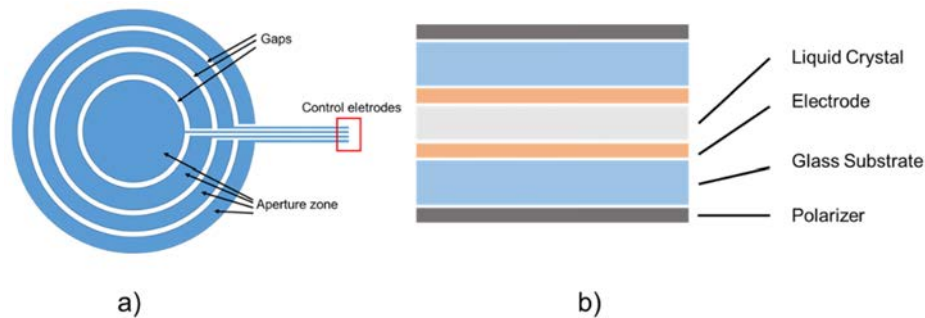


Fig. 5. (a) Design of the aperture patterns. (b) Liquid crystal device construction.

If there is no gap between the POSA element and the MFL surface, the radii of the circular aperture zones would be the same as the corresponding radii of the different focal segments of the MFL surface. However, the thickness of the glass substrate as described earlier introduced an unavoidable spacing between the POSA element and the multi-focal lens surface. Even though the spacing is only about 1.4mm, it introduces a slight aperture mismatch between the POSA and the MFL surface. Let us consider the central zone as an example and assume a small gap,  $g$ , between the POSA and the MFL surface, as illustrated in Fig. 6(a). An off-axis ray bundle illustrated in red rays enters the aperture of the POSA element. Due to the small gap, only a portion of the rays illustrated in purple color enters the aperture of the corresponding focal zone, while a small portion of the rays becomes stray light to an adjacent focal zone. As shown in the side view of Fig. 6(b), the red circle is the footprint of the ray bundle on the MFL surface after passing the patterned aperture, the blue circle is the corresponding aperture of the MFL surface, the purple-shaded area illustrates the footprint of the actual ray bundle that is properly focused, and the red-shaded area is the footprint of the stray-light rays. This effect will reduce the effective lens aperture and cause non-uniform image brightness across different zones, and the stray-light rays incident onto its adjacent focal zone will also lead to crosstalk and degradation of the image contrast.

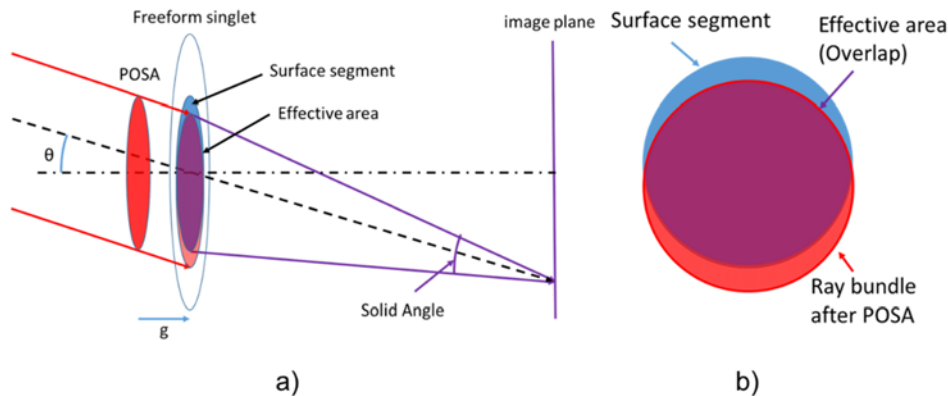


Fig. 6. (a) Illustration for calculating SA. (b) Effective area.

To account for the effect described above, the effects of the aperture sizes on the light throughputs of the different focal zone were analyzed by computing the solid angle variance of objects across a field of view (FOV) when imaged by different focal zones. An optimal set of aperture dimensions which yields a relatively constant illuminance for the different focal zones of the MFL singlet we designed (Fig. 2) is obtained and is listed in Table 1. It is worth noting that a small gap is made between adjacent aperture zones to provide a barrier for blocking stray light and to place electrodes. With the selected set of aperture dimensions, Fig.

7(a) plotted the solid angle of the on-axis image point through the four different focal zones as the spacing between the POSA and the MFL is increased from its minimal gap to 2 mm. The fairly constant solid angle through suggests that small gap between the POSA and MFL is tolerable. Figure 7(b) further plotted the solid angle variation as a function of FOV for the four different focal zones, which suggests that the variation of light throughput across the four focal zones is less than 30% for a FOV of  $\pm 20^\circ$ .

**Table 1. SLM aperture size configuration.**

Lens segment focal Length /mm	POSA aperture radius/mm	
	inner	outer
140	0	4.8
110	4.85	6.92
80	6.97	8.44
50	8.49	10

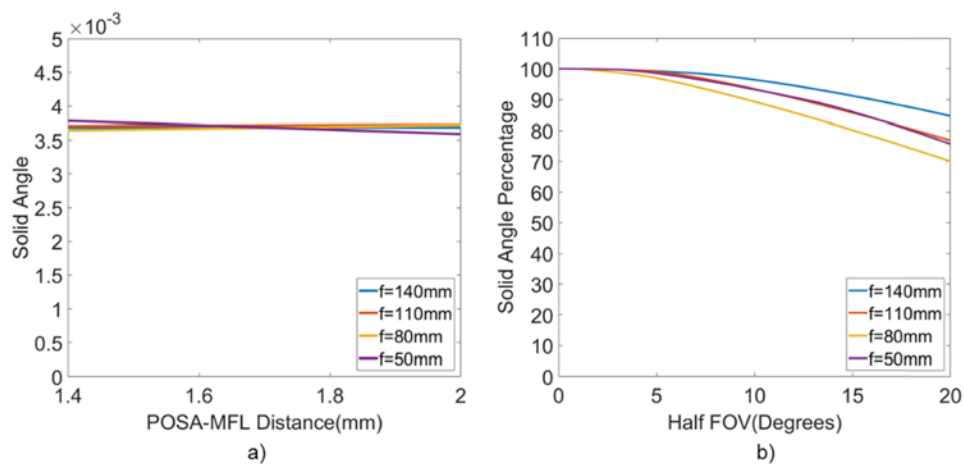


Fig. 7. Simulation results. (a) Relationship between solid angles of on-axis points and POSA-MFL distance for the four foci. (b) Solid angles of off-axis points at different FOV for the four focal zones when the POSA-MFL distance is 1.6mm.

Figure 8(a) shows the prototype of a liquid crystal based POSA fabricated by our collaborators at the University of Central Florida using the specifications in Table 1. The liquid crystal shutter was fabricated in the following steps: Positive photoresist S1813 (Shipley) was spin-coated at 3000 rpm for 1 minute to form a thin film on an ITO-coated glass substrate. The coated sample was pre-baked at  $115^\circ\text{C}$  for 1 minute. It was then subjected to 405-nm UV light through a patterned photomask to expose concentric rings with width being  $50\ \mu\text{m}$ . The substrate was post-baked at  $115^\circ\text{C}$  for 1 minute, and then immersed in developer 351 (diluted with water with 1:5 ratio) for 2 minutes to remove the exposed photo-resist. It was then immersed in 12 M hydrochloric acid for 1 minute to etch away the ITO in the developed region. The unexposed photoresist was subsequently removed with acetone rinse. After that, a patterned ITO and a non-patterned ITO substrate were spin-coated with a thin layer of polyimide at 3000 rpm for 30 s. The polyimide coated substrates were then baked at  $220^\circ\text{C}$  for 2 hours for imidization. They were rubbed and sealed to form a  $90^\circ$  twisted-alignment cell. The cell gap was controlled at  $3.0\ \mu\text{m}$  with spherical silica spacers and liquid crystal material LC-05 ( $\Delta n = 0.15$ ,  $\Delta\epsilon = 3.0$  at 514 nm,  $22^\circ\text{C}$ ) was infiltrated through capillary action. Polarizers were laminated on both sides of the cell with the transmission axis parallel to the adjacent LC director and thus the transmission axis were also crossed at  $90^\circ$ . Then the patterned POSA based on twisted nematic configuration was obtained. The four electrodes on the top substrate control the four patterned apertures separately. The electrode at

the bottom substrate is the common electrode which is connected to the ground during the driving process.

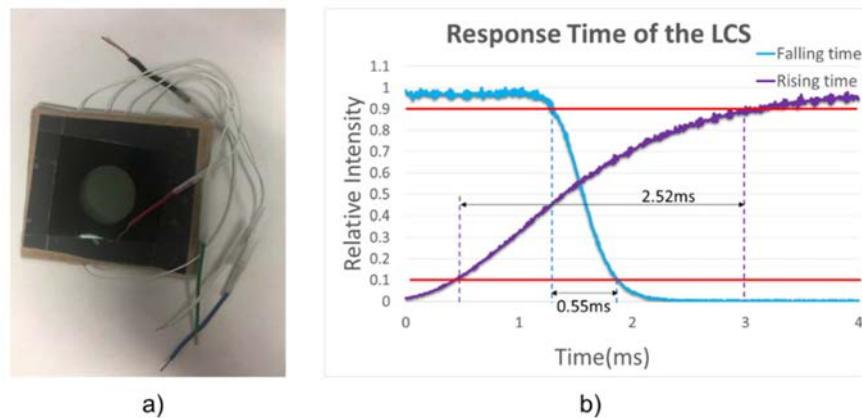


Fig. 8. (a) The picture of POSA. (b) Response time of the POSA.

Figure 8 (b) shows the test result for the response time of the POSA. We used 10% and 90% of the maximal transmittance as the threshold to define the on and off state of the shutter. From Fig. 8(b), we can see that the rising time for the transition of an aperture zone from being opaque to transparent is about 2.5 ms while the falling time for the inverse transition from being transparent to opaque is just about 0.5 ms, which is sufficient to switch among the four focal zones at an overall frequency of 400 Hz. The four different states of the POSA corresponding to the four different foci of the MFL are demonstrated in Fig. 9. Each state was controller by its own electrode. An aperture zone is set to be open with no voltage applied on its corresponding electrode, while it is set to be opaque with a 20 Vrms 2 kHz square wave applied.

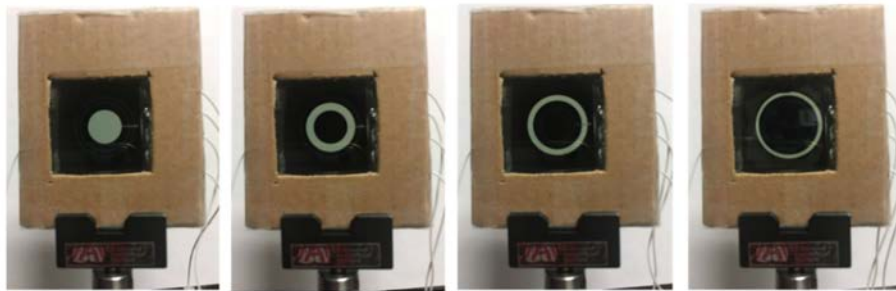


Fig. 9. Demonstration of the four states of the POSA.

#### 4. Experimental Results

To demonstrate the utility and performance of the proposed switchable MFL method, we built a simple imaging system using the MFL we designed along with catalog lenses. Figure 10 shows the schematic layout of our demo prototype, consisting of the POSA, the freeform MFL, two catalog lenses (L1 and L2), and a digital camera. The POSA is set adjacent to the freeform singlet. The different focal zones of the MFL form images of the objects at different depths (e.g. objects 1 and 2 in Fig. 10) at an intermediate image position. Lens L1 ( $f_1 = 80$  mm) is placed at the intermediate image position and serves as a field lens, while lens L2 ( $f_2 = 80$  mm) is placed at 80mm after L1 and serves as a collimation lens and the camera focus is always set at infinity. With such a configuration, the imaging system maintains a constant angular magnification for objects located at the different focal depths.

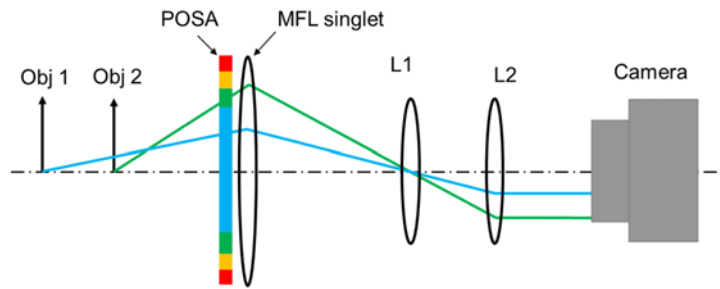


Fig. 10. Schematic layout of a multi-focal imaging system using a switchable multi-focal lens

Three printed bar targets were placed at 1000 mm, 339 mm and 157 mm, corresponding to the focal lengths of 140 mm, 110 mm and 80 mm, respectively. The targets are black-white gratings with 50/50 duty cycles and the periods of the gratings are chosen according to their corresponding distances so that each period of the three gratings subtends the same angular size to the system. Figure 11 shows the experimental setup with only one target object shown in the photo due to the large object distances of the other targets. Figures 12(a)-12(c) show the images of the three grating targets corresponding to the different focal length 140 mm, 110 mm, and 80 mm, respectively. We can see that for each focal length, the system can get a clear sharp image and the system maintained the same angular magnification and field of view across the different focal depths which is evidenced by the same grating period on captured image.

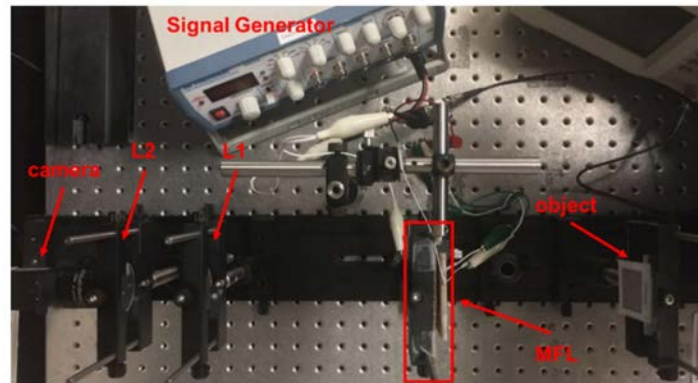


Fig. 11. Experimental setup of a MFL-based imaging system prototype

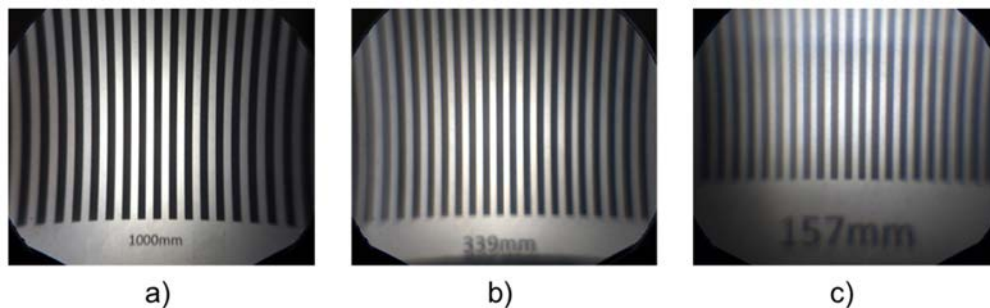


Fig. 12. Images of the three objects. a) Image distance = 1000 mm. b) Image distance = 339 mm. c) image distance = 157 mm

## 5. Conclusion

In this paper, we presented a new method of creating a digitally switchable multi-focal lens using freeform optics and liquid crystal technique, which offers the capability of rapidly switching the optical power of an imaging system among multiple foci. A custom-designed freeform four-foci lens with a clear aperture diameter of 20 mm and a custom-made high-speed programmable optical shutter array were demonstrated. The paper further demonstrated a proof-of-concept multi-focal imaging system prototype using the multi-focal lens and shutter array along with other catalog lenses. In the future, we will work on the optics system design for a compact, high frame rate, and high performance MFL with adequate number of focal planes suitable for many applications such as vari-focal or multi-focal head-mounted displays, microscopy, and endoscopy.

## Funding

Intel Corporation.

## Acknowledgments

This research was funded in part by a research gift by Intel Corporation. Dr. Hong Hua has a disclosed financial interest in Magic Leap Inc. The terms of this arrangement have been properly disclosed to The University of Arizona and reviewed by the Institutional Review Committee in accordance with its conflict of interest policies.